CORA Cork Open Research Archive
Cartlann Taighde Oscailte Chorcaí

Title	Simple rules for optimizing asymmetries in SOA-based Mach-Zehnder wavelength converters
Authors	Dailey, James M.;Koch, Thomas L.
Publication date	2009-04-24
Original Citation	Dailey, J.M., Koch, T.L. (2009) 'Simple Rules for Optimizing Asymmetries in SOA-Based Mach-Zehnder Wavelength Converters'. Journal of Lightwave Technology, 27 (11):1480-1488. doi: 10.1109/JLT.2009.2012875
Type of publication	Article (peer-reviewed)
Link to publisher's version	http://www.opticsinfobase.org/abstract.cfm?URI=jlt-27-11-1480 - 10.1109/JLT.2009.2012875
Rights	© 2009 IEEE. Personal use of this material is permitted. Permission from IEEE must be obtained for all other uses, in any current or future media, including reprinting/republishing this material for advertising or promotional purposes, creating new collective works, for resale or redistribution to servers or lists, or reuse of any copyrighted component of this work in other works.
Download date	2026-11-16 09:49:40
Item downloaded from	https://hdl.handle.net/10468/409



UCC
University College Cork, Ireland
Coláiste na hOllscoile Corcaigh



© 2009 IEEE. Personal use of this material is permitted. Permission from IEEE must be obtained for all other uses, in any current or future media, including reprinting/republishing this material for advertising or promotional purposes, creating new collective works, for resale or redistribution to servers or lists, or reuse of any copyrighted component of this work in other works.

J.M. Dailey and T.L. Koch, “Simple Rules for Optimizing Asymmetries in SOA-Based Mach-Zehnder Wavelength Converters”, *Journal of Lightwave Technologies*, **27** (11), pp 1480-88, 2009.

http://ieeexplore.ieee.org/search/srchabstract.jsp?tp=&arnumber=4840397&queryText%3Dj.m.+dailey%26openedRefinements%3D*%26filter%3DAND%28NOT%284283010803%29%29%26searchField%3DSearch+All

Simple Rules for Optimizing Asymmetries in SOA-Based Mach-Zehnder Wavelength Converters

J. M. Dailey, *Student Member, IEEE* and T. L. Koch, *Fellow, IEEE, Fellow, OSA*

***Abstract*—We present an analysis of semiconductor optical amplifier (SOA) based differential Mach-Zehnder wavelength converters with a specific focus on optimizing performance through intentional asymmetries in optical power splitting, SOA bias, and interferometer phase bias. By introducing a simple conceptual framework for understanding the amplifier pulse dynamics, two simple yet effective design rules are derived. These design rules are validated using pseudo-random code in a comprehensive computer model, demonstrating the performance penalties that result when attempting optimization using only unequal SOA biasing or phase biasing. This work illustrates that dramatic improvements in extinction and eye margin can be achieved with optimized splitter asymmetries, and has significant implications for improved network performance and converter cascadability.**

***Index Terms*—Optical Frequency Conversion, Optoelectronic devices, Optical Switches, Semiconductor Optical Amplifier**

I. Introduction

All-Optical wavelength conversion continues to attract considerable research interest for its potential to enable ultra-high-speed, low-cost, and efficient signal routing in wavelength-division-multiplexed networks. Semiconductor optical amplifiers (SOAs) have been key components in this research due both to their large nonlinearities, enabling switching at conventional communications power levels, and to their potential for monolithic integration in highly compact and stable modules[1, 2].

Various configurations have demonstrated conversion speeds beyond limits suggested by carrier recombination times, including discrete trailing filter [3], delayed interference [4] arrangements, and differential Mach-Zehnder designs [5-9] incorporating embedded SOAs. It has been generally observed in the latter that improved switching performance is achieved through some means of asymmetrical operation including unequal drive currents to the SOAs, unequal optical injections, and unequal relative phase biasing of the interferometer. However, no simple analytical design rules have emerged for selecting asymmetries in high-speed wavelength converters to maximize performance, perhaps due to the assumed complexity of nonlinear SOA-pulse dynamics and the resulting need for intensive numerical modeling to capture realistic device behavior.

In this paper we introduce a simple conceptual framework to understand the impact of design asymmetries based upon our observation that major performance degradations result from (1) quasi-static imbalance of phase and power which impacts extinction ratio, combined with (2) dynamic phase imbalance that produces trailing satellite pulses. We develop first-order design rules for optimized asymmetries that minimize these two deleterious effects, respectively, for long strings of "0" data bits and isolated "1" data bits. We then validate the efficacy of these design rules under more realistic operating conditions by employing pseudo-random code in a comprehensive numerical model for SOA dynamics, illustrating that dramatic relative increases in eye margins are achieved for optimized asymmetries. We summarize our results in the conclusion, which is followed by an appendix describing the computer model and a brief derivation of results used in the text. This work clearly illustrates the hazards of assuming that high performance can be achieved through optimized asymmetrical electrical and phase biasing alone, and provides prescriptive tradeoffs between the phase and optical injection asymmetries that are generally required to achieve optimized performance.

II. Wavelength Converter Operation

A typical differential Mach-Zehnder interferometer (MZI) wavelength converter [6] is shown above in Fig. 1. An unmodulated probe beam (λ_{probe}) enters a power splitter (β_{probe}), propagates through the SOA pair, and for non-inverting operation combines destructively at the output. The π phase difference needed for destructive interference at the converter output can be realized through a static phase shift (ϕ_0), asymmetrical SOA optical and current injections, or some combination of both. Optical data pulses (λ_{signal}) divide at

Manuscript received July 18, 2008. The authors gratefully acknowledge support by Alcatel-Lucent Bell Laboratories under the DARPA DOD-N IRIS project, and the state of Pennsylvania under BFTDA Grant ME#21-116-0014.

The authors are with the Center for Optical Technologies, Lehigh University, Bethehem, PA 18015 USA (email: jmd3@lehigh.edu and tlkoch@lehigh.edu).

β_{signal} and are injected into the SOAs. The data signal dynamically saturates the SOA and induces gain and phase deviations at λ_{probe} through nonlinear cross-phase modulation (XPM) and cross-gain modulation (XGM). An optical delay, τ, in the data signal path preceding SOA2 allows a data pulse to reach SOA1 first; XPM and XGM on the probe inside SOA1 disrupts the destructive interference at the MZI's symmetric output coupler and creates the rising edge of a pulse. The same process then occurs in the SOA2 path a time τ later, enabling SOA2 to rebalance the interferometer and re-establish the destructive interference for the falling edge of the output pulse at λ_{probe}. This switching window defines the converted data pulsewidth and allows the MZI converter to operate at bit-rates well beyond what would be possible using only the SOA's relatively slow phase recovery. In fact, though we have modeled a 40 Gb/s wavelength converter throughout this paper, we believe that the design rules we develop should work reasonably well in >100 Gb/s systems.

To accurately model SOA-based wavelength converter performance, we employ a comprehensive numerical traveling wave SOA model, outlined in Appendix A, that includes hot-carrier dynamics and rigorously calculates the phase response without invoking an α-factor approximation [10]. As an example of the utility of our model, Fig. 2 illustrates the impact that a static phase shift has on the converter performance when symmetrical power splitters are used, i.e. $\beta_{probe} = \beta_{signal} = 0.5$. Figs. 3a and 3b depict the MZI output with a 40 Gb/s return-to-zero (RZ) input data signal consisting of 8 ps pulses in a 2^7-1 pseudo-random bit sequence (PRBS). At each value of ϕ_0, the relative SOA injection currents have been reset to obtain the optimum output eye at λ_{probe}, characterized by both the extinction X, where

$$X \equiv 10 \cdot \log_{10}\left(P^1_{avg} \big/ P^0_{avg}\right)$$

and opening O, where

$$O \equiv \left(P^1_{\min} - P^0_{\max}\right) \big/ \left(P^1_{avg} - P^0_{avg}\right)$$

The opening O captures the impact of pattern effects, whereas the extinction ratio X is sensitive to DC offsets to which O is relatively insensitive. The power levels used to calculate X and O are defined in Fig. 3b and the data input parameters are X_{input}=42 dB and O_{input}=0.99.

To generate the data in Figs. 2-3, the current into one of the SOAs is dropped until a total relative phase shift of ~π is attained; the eye degradation is most dramatic when ϕ_0=0 and the phase shift is achieved solely through asymmetrical SOA current injections. The poor extinction ratio is due to the impossibility of providing both equal output powers and a π phase shift on the probe output leading to incomplete destructive interference.

The use of a static phase shift allows the probe powers to balance and substantially improves both the eye extinction and opening, though significant degradation due to ringing and pattern effects remain, and would clearly lead to performance penalties even when received by a detector with bandwidth optimized for 40 Gb/s.

Origins of the poor eye performance are further elucidated in Fig. 4 which contains temporal plots of the two SOA phase responses. The probe phase shifts arise from signal-induced XPM, with the transmission window opening due to the saturation of SOA1 from the data pulse. When SOA2 is saturated to shut the transmission window, SOA1 has partially recovered and the different SOA phases and gains lead to imperfect destructive interference manifested through the emergence of trailing satellite pulses [11] and reduced extinction. Changes in SOA bias can only be used to trade-off between these two effects, leading to the relatively poor eyes in Fig. 3 which illustrate results with the best possible combination of SOA current injections.

The strong impact of ϕ_0 on converters with symmetrical splitters suggests that either precise fabrication control of intentional phase delay, or some form of active phase control, is desirable. However, even at the optimum there is > 1.2dB penalty in eye opening. This clearly illustrates that an MZI converter design incorporating symmetrical 3 dB power splitters produces a relatively poor output eye, even with a nominal π static phase shift inside the interferometer. The use of optical filters [3, 12-14] is likely to have contributed to the favorable performance of earlier reports of symmetrically designed MZI converters [5].

We will now show that *power* asymmetries in the probe and signal paths, rather than phase asymmetries, can be used to both maximize the DC extinction for an arbitrary ϕ_0 as well as eliminate satellite pulses by enabling matched outputs in spite of SOA1's partial recovery. Furthermore, the dependence of the output eye on the static phase shift is shown to be significantly reduced.

We do not explicitly evaluate polarization dependencies here, which effectively implies single polarization operation or polarization-indedendent modal gain. Polarization-dependent modal gain coupled with different polarization inputs in the system would result in polarization dependence in the ideal power splitter designs. If there were drifting input polarizations, this would lead to a performance penalty, but we show later in Figs 6b and 7c that this system is fairly robust against minor deviations from ideal operating conditions and splitter design values.

The following section describes a simplified conceptual picture of how the optimization of the MZI converter can be achieved through the design of the power splitters, and demonstrates through the numerical model the dramatic performance improvements that can result.

III. POWER SPLITTER DESIGN

Based upon the observations above, the asymmetries in data

and probe splitters should be chosen such that (A) with no input data signal, the two probe SOA outputs are equal in amplitude and obtain a π relative phase offset from each other, and simultaneously (B) the phase and gain responses of the two SOAs properly align in amplitude during recovery to eliminate trailing satellite pulses [4, 15, 16].

To achieve condition (A), we can use static SOA device characteristics to determine the proper splitting of input probe power β_{probe}. For a given output from one of the SOAs, for example, we would need to vary both the input power and the drive current to that SOA in such a way as to achieve an output that perfectly balances the output from the other for destructive interference. If we adjust the current to maintain *constant SOA output power* while the input optical power varies, it is shown in Appendix B that the phase deviation $\delta\varphi$ with SOA input power P_{in} will vary according to (1) below

$$\frac{d\delta\varphi}{dP_{in}} = -\frac{\alpha}{2}\frac{1}{P_{in}} \tag{1}$$

Here $\delta\varphi$, P_{in}, and α are the probe SOA output phase, probe SOA input power, and linewidth enhancement factor, respectively. Integrating (1), we seek the pair of probe input powers that yields the π phase shift needed to meet optimization condition (A)

$$\begin{aligned} \delta\varphi_2 - \delta\varphi_1 = -\pi + \phi_0 = -\frac{\alpha}{2}\ln\frac{P_{in,2}}{P_{in,1}} \\ \rightarrow \quad \frac{P_{in,2}}{P_{in,1}} = e^{\frac{2}{\alpha}(\pi-\phi_0)} \end{aligned} \tag{2}$$

where $0 \le \phi_0 \le \pi$. Solving for β_{probe}, yields

$$\begin{aligned} \beta_{probe} \equiv \frac{P_{in,1}}{P_{in,1}+P_{in,2}} &= \frac{1}{1+\frac{P_{in,2}}{P_{in,1}}} \\ &= \frac{1}{1+e^{\frac{2}{\alpha}(\pi-\phi_0)}} \end{aligned} \tag{3}$$

where a $\beta_{probe} < 0.5$ indicates a smaller optical injection into SOA1. The –π in (2) results from our choice that the nominal operation of SOA2 has a smaller current and higher optical injection. The space switch analysis in [17] is consistent with (3) under different design constraints, and (3) is applied here as a proposed optimization for the the high-speed MZI wavelength converter.

We attempt to achieve optimization condition (B) through the selection of β_{signal} to ensure the best scaling of phase and gain responses for proper temporal alignment during recovery. For this simple optimization argument, we ignore any differences in temporal gain and phase recovery behavior and focus on balancing the phase excursion which can be expected to impact satellite pulses to a greater degree. The impact of this simplification will be implicitly evaluated at 40 Gb/s through our numerical simulations which inherently include significant differences in gain and phase recovery. For example, some dissimilarity in the temporal behaviors of the gain and phase recoveries is expected simply due to the exponential behavior of gain for a given imaginary index excursion, but also from the detailed impact of ultrafast dynamical effects such as carrier-heating that are included in the numerical model [10].

If we denote the phase excursion of an SOA induced by a signal pulse as $\Delta\phi$, then the two phase excursions should be equal at t = τ (the optical delay preceding SOA2). The relative magnitudes of the phase excursions should then be governed by a ratio denoted as η_0 which is given by

$$\frac{\Delta\phi_2}{\Delta\phi_1} = e^{-\frac{\tau}{0.46\,\sigma}} \equiv \eta_0 \tag{4}$$

where the SOA recovery is modeled as a simple exponential for this qualitative discussion, and σ is the 10% to 90% exponential recovery time constant which is assumed equal for both SOAs.

$G_{1,2}$ and $\Delta\phi_{1,2}$ are the gain minima and phase deviations due to the signal pulse, respectively, and are shown in Fig 5. They relate through the α-factor according to

$$\Delta\phi_1 = \frac{\alpha}{2}\cdot\ln\frac{G_1}{G_{01}} \tag{5}$$

where G_{01} is the steady-state gain preceding the signal pulse in SOA1. The ratio of phase changes is then

$$\eta \equiv \frac{\Delta\phi_2}{\Delta\phi_1} = \frac{\alpha_2\ln\{G_2/G_{02}\}}{\alpha_1\ln\{G_1/G_{01}\}} \cong \frac{\ln\{G_2/G_{02}\}}{\ln\{G_1/G_{01}\}} \tag{6}$$

and β_{signal} must be chosen so that $\eta \cong \eta_0$ or

$$\eta = \frac{\ln\{G_2/G_{02}\}}{\ln\{G_1/G_{01}\}} \cong e^{-\frac{\tau}{0.46\,\sigma}} = \eta_0 \tag{7}$$

Memory effects will clearly lead to a variation in η across different bit sequences, but in this work we postulate that good optimization can be achieved by evaluating (7) following the injection of an isolated one-bit into the SOA pair. The SOA gain ratios contained in (7) are easily measured on a high-bandwidth oscilloscope, and this equation gives a clear picture of the rationale for the asymmetry. As stated earlier, the gain and phase recoveries are not identical, and the recovery rates

are not truly exponential as they generally depend on the SOA operating conditions. Despite these qualifications, we demonstrate in the next section that σ, and thus η_0, are relatively constant across a large span of input powers and bias currents, allowing for good optimization with a fixed splitting ratio β_{signal}.

IV. NUMERICAL CONFIRMATION

The key results from the preceding section are (3) and (7), and their utility is now evaluated in a realistic operating scenario using a comprehensive SOA computer model. Appendix A contains a description of the model along with the SOA device parameters. The optical and electrical bias points must be selected so that the probe outputs are equal in power and together with the static phase shift, ϕ_0, obtain a π relative phase shift. To determine these operational points, a probe beam at 1547nm is injected into the SOA and its output power and phase are calculated for various input powers and current biases with zero data signal injection.

Fig. 6a illustrates the evolution of the output phase with input power, where at each point the current bias has been adjusted to maintain a constant output power. In this way, Fig. 6a is a graphical depiction of the behavior predicted by the simple model captured in (1). Noting that the probe input power is plotted logarithmically and normalized, (1) is rewritten

$$\begin{aligned}\delta\varphi &= -\frac{\alpha\ln(10)}{20\pi}\left\{10\cdot\log_{10}\frac{P_{in}}{0.001}\right\} \quad + \quad C_0 \\ &= -\frac{\alpha\ln(10)}{20\pi}\cdot P_{in,dBm} \quad + \quad C_0\end{aligned} \tag{8}$$

where C_0 is an integration constant of no consequence.

A linear fit of $\delta\varphi$ vs. $P_{in,dBm}$ indicates a slope of ≅ -0.17, which corresponds to an α of 4.6. While the model does not use an α-factor approximation in its calculations, the nearly constant slope of $\delta\varphi$ in Fig. 6a indicates that for this static consideration the effective α behavior across the operational regime is constant, suggesting that a static β_{probe} will work well across a wide range of input powers. The α of 4.6 is also quite typical for experimental values of bulk SOAs as modeled here. Using this value for α and setting ϕ_0 to zero, (3) indicates β_{probe} = 0.2, i.e. a 20/80 power coupler should be utilized at the probe input along with appropriate bias currents. Fig. 6b contains the results from a more extensive sampling of the parameter space and illustrates the variation of the probe DC extinction with β_{probe}. The plot indicates a typical interferometer-like transfer function, and even a variation of as much as ~25% in β_{probe} allows for an extinction of at least -30dB.

Because α will have some probe wavelength dependence, the ideal β_{probe} will vary according to the α variation as captured in (3). For a fixed β_{probe}, this wavelength variation can be accomodated to a limited extent through the adjustment of SOA bias currents, though this also unbalances the output powers. For large variations in probe wavelengths, a dynamically adjustable power splitter [18] or phase bias [16] could be advantageous in restoring the equalized output powers and π phase offsets.

To achieve condition (B), β_{signal} is chosen so that (7) is satisfied. A numerical experiment was executed to evaluate the left hand side of (7), and condition (A) is maintained by choosing β_{probe} = 0.2 while the SOA current biases are chosen to maximize DC extinction. The resultant SOA states are SOA2 @ (347 mA/-8.8 dBm) (i.e. input current/input power) and SOA1 @ (360 mA/-14.6 dBm) and the probe wavelength is still 1547nm. An isolated 8ps pump pulse at 1567nm is injected into each SOA and the resultant peak gain excursions at 1547 nm were calculated. η was thus modeled over a range of signal input powers and demonstrated good agreement when compared with the actual phase change ratios calculated in the model.

The phase recovery time (σ) of the 1547 nm probe must be known in order to evaluate the right side of (7). While this would be measured experimentally in a real device, Fig. 7a tabulates the results of a phase recovery fitting in our numerical model spanning a large range of data input pulse powers and SOA operating points. The variation of σ is seen to be relatively small and a representational value of ≅ 28ps is chosen to evaluate (7) yielding η_0 ≅ 0.5. With this value of η_0, condition (B) dictates that β_{signal} be adjusted so as to achieve η ≅ 0.5 on the left side of (7). While it is not clear *a priori* that a fixed value of β_{signal} can achieve this over a useful range of input powers, Fig. 7b illustrates the numerically evaluted variation of β_{signal} required to achieve a given value of η as a function of total signal input power. It can be seen that for η=0.5, a signal splitting of β_{signal} = 0.5 yields a good approximation to the desired phase excursion scaling over a broad range of input powers. Fig. 7b also clearly indicates that η does vary with input power, which is expected given the asymmetrical optical and electrical injections. Variance can also be expected with input wavelengths leading to some violation of the criterion denoted in (7), but given a static β_{signal}, some accomodation to (7) could be realized by dynamically tracking the SOAs' current biases and the total probe input power to the MZI.

The sensitivity of the choice of β_{signal} is evaluated by varying the peak signal power into SOA2 and adjusting I_2 to optimize the output eye parameters *X* and *O*. The results are shown in Fig. 7c which indicates a full-width half maximum (FWHM) for *X* of ~35% of β_{signal}. Furthermore, our choice of β_{signal}=0.5 sits in a sweet spot between the maxima for *X* and *O*.

The computer model is then used to evaluate the efficacy of the splitter asymmetries based upon the simple design rules above. The same numerical experiment carried out earlier to evaluate the output eye performance as a function of static phase shift is repeated for these asymmetrical MZI designs, but

now the two power splitters are optimized for each of the static phase shifts according to the design rules given by (3) and (7). Examples of the resulting operational parameters are summarized in Table I, which provides selected values of the design parameters for near-ideal eye performance at a given static phase shift. The probe and signal wavelengths remain λ_{probe} = 1547nm and λ_{signal} = 1567nm and the same 2^7-1 PRBS word is used to evaluate the eye extinction (*X*) and opening (*O*) at the converted output.

TABLE I
ASYMMETRICAL DESIGN PARAMETERS

ϕ_0	β_{probe}	β_{signal}	I_1	I_2
0	0.20	0.5	361	340
$\pi/4$	0.27	0.57	361	341
$\pi/2$	0.34	0.63	361	345
$3\pi/4$	0.42	0.66	361	352
π	0.5	0.71	361	360

To illustrate that these actually provide improved eye diagrams in a realistic pseudo-random code application, Fig. 8 illustrates the results of the numerical experiment and captures several of the key conclusions of this paper. Fig. 8 shows the variation of *X* and *O* as a function of the static phase shift, ϕ_0, for three different scenarios and constraints. The data displayed by the dotted line is borrowed from Fig. 2, and shows the eye variation for a converter with symmetrical power splitters and currents optimized at each point. The solid line shows the best eye performance for an MZI with asymmetrical power splitters *redesigned at each value* of ϕ_0 according to the simple design rules, and are in accordance with Table I. These results show clearly that $\beta_{probe} < 0.5$ provides improved performance as predicted. Since practical devices may include a fixed value of β_{probe}, Fig. 8 also shows in the dash data how a *fixed probe splitting* of β_{probe} = 0.34, which is nominally optimized for a static phase shift of $\phi_0=\pi/2$, behaves for other values of static phase shift ϕ_0.

Fig. 9 shows the best output eye for a converter with asymmetrically optimized power splitters for the particular case of a static phase shift of ϕ_0=0. The results are slightly better at other static phase shifts, but essentially indistinguishable as long as the properly selected asymmetrical splitter values are used according to (3) and (7). The optimized eye clearly demonstrates a dramatic improvement in extinction, opening, and suppression of satellite pulses, with an eye opening penalty below 0.25 dB with respect to unity. This should be compared with the best eyes using symmetrical splitters provided in Fig. 2.

When comparing the symmetrical (dotted) and the asymmetrically continuously optimized (solid) converter data curves, the largest performance enhancement occurs at ϕ_0=0 with 21.5 and 4.6 dB improvements in the extinction and opening, respectively. The difference narrows as ϕ_0 approaches π, but significant improvements of 12 and 1.5 dB for *X* and *O* are still realized with the asymmetrical splitters.

The curve displaying the behavior of a converter with a fixed value of β_{probe} = 0.34, which was optimized for $\phi_0=\pi/2$ (dash), also demonstrates a favorably decreased sensitivity of the eye opening to changes in the static phase shift, with even the most severe penalty in *O* being below 0.7dB over the entire range. Of course, at its optimum point it produces a very small penalty of < 0.3dB relative to unity. This curve, with fixed asymmetric β_{probe}, also maintains at least 10dB extinction over the entire range of ϕ_0.

These observations lead us to the major conclusions of this paper: (1) *static optical phase shifts alone will not necessarily produce an optimized eye*, and (2) *converters with proper choice of splitter asymmetries provide outstanding performance without the need for perfectly optimized static phase shifts.* In particular, a significant penalty in both *X* and *O* will be incurred if symmetrical power splitters are used, regardless of the phase shift utilized in the MZI, while a design with optimized splitter asymmetry will produce outstanding eyes at the design static phase shift but also very good eyes at other values of static phase shift.

V. Conclusions

We have demonstrated the poor wavelength converter performance that can arise when utilizing 3-dB power splitters in a Mach-Zehnder configuration, and that these degradations are only partially mitigated through the use of static phase shifts. The utilization of a few simple and well-known SOA approximations has enabled us to derive two compact equations leading to the design of more appropriate asymmetrical power splitters for both the input probe and signal beams. A comprehensive computer model was used to validate these design principles with realistic pseudo-random code. We have also shown that proper choice of splitter asymmetries can result in dramatic improvements in eye quality with diminished dependence on static phase shift. The resulting eye quality, as illustrated for example by Fig. 9, clearly carries the potential for significant improvements in network performance and also converter cascadability.

We have not explicitly examined here the wavelength sensitivities of the power splitter designs, which we expect to manifest primarily through the wavelength dependence of both the dynamic amplitude phase coupling (usually captured through the α-factor) and the XPM phase shifts. We used our numerical model to estimate the changes in $\alpha(\lambda)$ across the C-band, which were then inserted into (3) to calculate the variation in β_{probe}. A comparison of this variation with the

results in Fig. 6b suggests that the optimized splitter design should provide fairly robust DC extinction with wavelength change. Gain changes with wavelength will also affect the choice of β_{signal}, though the results in Figs 7a-c also suggest resistance to the potential performance degradation from this effect. The incorporation of dynamical power splitters or phase bias could aid in the wavelength tunability of this system.

ACKNOWLEDGMENT

The authors wish to thank colleagues at Alcatel-Lucent Bell Laboratories, and Jesse Simsarian in particular, for helpful discussions and ideas that have contributed to this work.

APPENDIX A
COMPUTER MODEL

A computer model is used to characterize the SOAs' behavior and validate the design principles proposed in the preceding treatment. A 40 Gb/s system is characterized through the implementation of a bulk-SOA traveling wave rate equation model including ultrafast effects due to carrier heating [10, 19]. The material gain is calculated using a density matrix approach which eliminates various linearizing approximations, e.g. the α-factor. The isotropic complex refractive index calculated from the density matrix model is given by:

$$\tilde{n}(\omega) = \frac{\mu_{cv}^2}{4\pi\varepsilon_0 n}\left(\frac{2m_r}{\hbar^2}\right)^{3/2} \cdot \int_0^\infty \left(f_e + f_h - 1\right)\sqrt{\hbar\Omega}\,\frac{\left[-i\cdot\frac{1}{\pi}T_2 + \frac{1}{\pi}\left(\omega - \frac{E_g}{\hbar} - \Omega\right)T_2^2\right]}{1+\left(\omega - \frac{E_g}{\hbar} - \Omega\right)^2 T_2^2}\,d\Omega \tag{A1}$$

The imaginary part of (A1) corresponds to the material gain while the real part contains the contribution to the refractive index of the resonant band-to-band transitions. T_2 is the dephasing time, while ω, μ_{cv}, m_r , n, and E_g represent the optical angular frequency, dipole matrix element, reduced mass, background (non-resonant) refractive index, and bandgap energy respectively. f_e and f_h are the Fermi-Dirac occupational probabilities for electrons and holes. The rate equations are shown below.

$$\left(\frac{\partial}{\partial t} \pm v_g\frac{\partial}{\partial z}\right)S_\omega^{\pm} = v_g\Gamma S_\omega^{\pm}\left(g_\omega - \alpha_{FC}N - \alpha_0\right) + R_{sp,\omega} \tag{A2}$$

$$\left(\frac{\partial}{\partial t} + v_g\frac{\partial}{\partial z}\right)\delta\varphi_\omega = -v_g\Gamma\frac{\omega}{c}\left(\delta n_{b-b,\omega} + \delta n_{plasma,\omega}\right) \tag{A3}$$

$$\frac{dN}{dt} = \frac{I}{qV} - v_g\sum_\omega g_\omega\cdot\left[S_\omega^{+} + S_\omega^{-}\right] - AN - BN^2 - CN^3 \tag{A4}$$

$$\frac{dT}{dt} = \frac{1}{\frac{\partial U}{\partial T}}\cdot\left(\frac{dU}{dt} - \frac{\partial U}{\partial N}\frac{dN}{dt}\right) - \frac{T - T_0}{\tau} \tag{A5}$$

Equation (A2) describes the evolution of the forward and reverse propagating signals as well as the amplified spontaneous emission (ASE) photon density, S, where v_g, Γ, g_ω, and α_0 are the group velocity, waveguide confinement factor, frequency-dependent material gain, and passive waveguide loss, respectively. Free-carrier and inter-valence band (IVB) absorption are captured in α_{FC} and $R_{sp,\omega}$ is the spontaneous emission rate, described below

$$R_{sp,\omega} = \frac{2\Gamma^2\cdot g'\cdot\Delta\omega}{2\pi\cdot A_{act}} = \frac{2\Gamma^2\cdot n_{sp}g\cdot\Delta\omega}{2\pi\cdot A_{act}} \tag{A6}$$

where A_{act} and $\Delta\omega$ are the active region area and the spectral width of the ASE calculation, respectively. g' and g'' are the stimulated emission and absorption components of the gain, calculated from (A1), where $g = g' - g''$ [20]. n_{sp} is the commonly used spontaneous emission factor. ASE has been included to accurately capture the saturation dynamics, and so a high spectral resolution is unnecessary. $\Delta\omega$ is split into three wavelength regions centered on the ASE peak. ASE has been excluded from the output eye calculations.

The forward-propagating signal phase is described in (A3) with terms for the frequency-dependent refractive index changes due to the dipole band-to-band transition ($\delta n_{b\text{-}b}$) and the plasma (δn_{plasma}). $\delta n_{b\text{-}b}$ is calculated using (A1) and the Drude model is used to calculate δn_{plasma} [21]

$$\delta n_{plasma} = \frac{-\lambda^2 q^2 N}{8\pi^2\varepsilon_0 n c^2 m_r} \tag{A7}$$

where λ, q, N, ε_0, and c are the optical wavelength, electron/hole charge, carrier density, permittivity of free space, and the speed of light, respectively.

The carrier density changes are described in (A4) which contains terms for the electrical current, I, cavity volume, V, as well as the linear, bi-molecular, and Auger recombination coefficients denoted by A, B, and C, respectively.

Carrier heating is captured in (A5) using a carrier temperature rate equation, where U is the carrier plasma

energy density. The plasma-phonon interaction is expressed in the phenomenological addition to the r.h.s. of (A5) which describes the restoration of the carrier temperature to that of the lattice temperature, T_0, with the time constant τ. The temperature for electrons and holes, as well as their density, are assumed to be equal at all times. The dU/dt term is evaluated using a simple expression for the rate of energy change from stimulated emission as well as free carrier and IVB absorption

$$\frac{dU}{dt} = -\sum_i (\hbar\omega_i - E_g) v_g g_{\omega_i} (S^+_{\omega_i} + S^-_{\omega_i}) + \sum_i \hbar\omega_i v_g \alpha_{FC} N (S^+_{\omega_i} + S^-_{\omega_i}) \quad \text{(A8)}$$

The summation is used to include contributions from all relevant optical frequencies.

The remaining derivatives on the r.h.s. of (A5) are evaluated using the relationship between the energy density and the carrier distributions

$$U = \frac{2}{\sqrt{\pi}} kT\left[N_c F_{3/2} + P_v F_{3/2}\right] \quad \text{(A9)}$$

where N_c and P_v are the effective density of states expressions for the conduction and valence bands, and $F_{3/2}$ is the Fermi-Dirac integral of order 3/2 [22].

Our initial modeling with spectral hole burning suggested its overall impact to be relatively inconsequential and it was eliminated from further calculations. Typical parameters for an InGaAsP SOA [20, 22] were used and are shown in Table II.

TABLE II
MODELING PARAMETERS

Symbol	Description	Value	
n	Background refractive index	3.4	
α_{FC}	Free carrier absorption	$2\cdot10^{-21}$	m^2
A	Linear recombination	$2\cdot10^{8}$	s^{-1}
B	Bi-molecular recombination	$6\cdot 10^{-16}$	m^3s^{-1}
C	Auger recombination	$8\cdot10^{-41}$	m^6s^{-1}
E_g	Bandgap	0.775	eV
m_e	Electron effective mass	$0.045\cdot m_0$	
m_h	Hole effective mass	$0.37\cdot m_0$	
μ_{cv}	Dipole matrix element	$10\cdot 10^{-29}$	C· m
T_2	Dephasing time	$150\cdot 10^{-15}$	s
τ	Temperature recovery time	$1.5\cdot 10^{-12}$	s
α_0	Carrier independent absorption	12000	m^{-1}
L	Device length	$2.0\cdot 10^{-3}$	m
Γ	Confinement factor	0.54	
V	Active region volume	$6\cdot 10^{-16}$	m^3
R	Facet reflectivity	0.0	
$\Delta\omega$	ASE Spectral Width	$4\cdot 10^{13}$	rad/s

These equations are solved on a space-time grid using the method of characteristics in conjunction with a fourth order Runge-Kutta solver implemented in Matlab. An injection current of 350 mA produces a gain peak around ~ 1548 nm of ~ 32 dB. The 3 dB bandwidth for the gain stretches over ~ 20nm and a 1547 nm signal quickly saturates the gain at an input power of -23 dBm, indicating the ease with which this SOA can be saturated and operated in the nonlinear regime. All optical splitters and couplers are assumed loss-less and wavelength-independent. The SOA output optical power (P) is calculated from the photon density (S), and the MZI output is calculated as

$$\frac{1}{2}\cdot\left|\sqrt{P_1}\cdot e^{i\cdot\delta\varphi_1} + \sqrt{P_2}\cdot e^{i\cdot\delta\varphi_2}\right|^2 \quad \text{(A10)}$$

where, for example, P_1 and $\delta\phi_1$ are the output power and signal phase from SOA1.

APPENDIX B

In the absence of a data input signal, the probe output power P_{out} is static and is given by

$$P_{out} = e^{\Gamma\int_0^L g\,dz} P_{in} \quad \text{(B1)}$$

If P_{in} varies but the current is maintained such that the output P_{out} is unchanged, then along such an operating curve we must have

$$\begin{aligned}\frac{dP_{out}}{dP_{in}} &= 0 \\ &= \frac{dP_{in}}{dP_{in}}\cdot e^{\Gamma\int_0^L g\,dz} + P_{in}\,\Gamma\int_0^L \frac{dg}{dP_{in}}dz\cdot e^{\Gamma\int_0^L g\,dz} \\ &= e^{\Gamma\int_0^L g\,dz}\left(1 + P_{in}\,\Gamma\int_0^L \frac{dg}{dP_{in}}dz\right)\end{aligned} \quad \text{(B2)}$$

and thus

$$\frac{-1}{P_{in}} = \Gamma\int_0^L \frac{dg}{dP_{in}}dz \quad \text{(B3)}$$

However, we can express the last integral in this expression as follows:

$$\Gamma\int_0^L \frac{dg}{dP_{in}}dz = -\Gamma\int_0^L \frac{4\pi}{\lambda}\frac{dn_{imag}}{dP_{in}}dz$$
$$= \frac{-1}{\alpha}\cdot\Gamma\int_0^L \frac{4\pi}{\lambda}\frac{dn_{real}}{dP_{in}}dz \qquad \text{(B4)}$$
$$= \frac{2}{\alpha}\cdot\frac{d\delta\varphi}{dP_{in}}$$

and we have

$$\frac{d\delta\varphi}{dP_{in}} = -\frac{\alpha}{2}\frac{1}{P_{in}} \qquad \text{(B5)}$$

where $\alpha \equiv \frac{\Delta n_{real}}{\Delta n_{imag}}$ is the usual α factor.

REFERENCES

[1] S. J. B. Yoo, "Wavelength conversion technologies for WDM network applications," *J. Lightw. Technol.,* vol. 14, no. 6, pp. 955-966, 1996.

[2] T. Durhuus, B. Mikkelsen, C. Joergensen, S. Lykke Danielsen, and K. E. Stubkjaer, "All-optical wavelength conversion by semiconductor opticalamplifiers," *J. Lightw. Technol.,* vol. 14, no. 6, pp. 942-954, 1996.

[3] Y. Liu*, et al.*, "Error-free 320-Gb/s all-optical wavelength conversion using a single semiconductor optical amplifier," *J. Lightw. Technol.,* vol. 25, no. pp. 103-108, 2007.

[4] J. Leuthold*, et al.*, "100 Gbit/s all-optical wavelength conversion with integrated SOA delayed-interference configuration," *Electron Lett.,* vol. 36, no. 13, pp. 1129-1130, 2000.

[5] C. Joergensen*, et al.*, "Wavelength conversion by optimized monolithic integrated Mach-Zehnder interferometer," *IEEE Photon. Technol. Lett.,* vol. 8, no. 4, pp. 521-523, 1996.

[6] P. Bernasconi*, et al.*, "Monolithically integrated differential Mach-Zehnder filter for 40 Gb/s wavelength conversion in high-confinement butt-joint SOAs," in *2006 International Conference on Indium Phosphide and Related Materials Conference Proceedings*, 2006, 241-243.

[7] M. L. Masanovic*, et al.*, "Widely tunable monolithically integrated all-optical wavelength converters in InP," *J. Lightw. Technol.,* vol. 23, no. 3, pp. 1350-1362, 2005.

[8] F. Ratovelomanana*, et al.*, "An all-optical wavelength-converter with semiconductor optical amplifiers monolithically integrated in an asymmetric passive Mach-Zehnder interferometer," *IEEE Photon. Technol. Lett.,* vol. 7, no. 9, pp. 992-994, 1995.

[9] S. Nakamura, S. Nakamura, Y. Ueno, and K. Tajima, "Error-free all-optical demultiplexing at 336 Gb/s with a hybrid-integrated symmetric-Mach-Zehnder switch," in *2002 OFC Proceedings*, 2002, FD3-1-FD3-3.

[10] J. M. Dailey and T. L. Koch, "Impact of carrier heating on SOA transmission dynamics for wavelength conversion," *IEEE Photon. Technol. Lett.,* vol. 19, no. 14, pp. 1078-1080, 2007.

[11] J. Sakaguchi, M. L. Nielsen, T. Ohira, R. Suzuki, and Y. Ueno, "Observation of small sub-pulses out of the delayed-interference signal-wavelength converter," *Jpn. J. Appl. Phys.,* vol. 44, no. 42-45, pp. L1358-L1360, 2005.

[12] J. Leuthold*, et al.*, "All-optical wavelength conversion using a pulse reformatting optical filter," *J. Lightw. Technol.,* vol. 22, no. 1, pp. 186-192, 2004.

[13] M. L. Nielsen, B. Lavigne, and B. Dagens, "Polarity-preserving SOA-based wavelength conversion at 40Gbit/s using bandpass filtering," *Electron Lett.,* vol. 39, no. 18, pp. 1334-1335, 2003.

[14] M. L. Nielsen and J. Mørk, "Increasing the modulation bandwidth of semiconductor-optical-amplifier-based switches by using optical filtering," *J. Opt. Soc. Am. B,* vol. 21, no. 9, pp. 1606-1619, 2004.

[15] Y. Ueno, "Theoretically predicted nonlinear phase imbalance requirement for delayed-interference signal-wavelength convertors (DISC)," *Jpn. J. Appl. Phys.,* vol. 43, no. 5B, pp. L665-L668, 2004.

[16] S. Kumar, B. Zhang, and A. E. Willner, "Impact of operational parameters on optimum performance of SOA-based differential-mode wavelength converters," *IEEE Photon. Technol. Lett.,* vol. 19, no. 19, pp. 1538-1540, 2007.

[17] J. Leuthold*, et al.*, "All-optical space switches with gain and principally ideal extinction ratios," *IEEE J. Quantum Electron.,* vol. 34, no. 4, pp. 622-633, 1998.

[18] N. S. Lagali, M. R. Paiam, R. I. MacDonald, K. A. W. K. Worhoff, and A. A. D. A. Driessen, "Analysis of generalized Mach-Zehnder interferometers for variable-ratio power splitting and optimized switching," *J. Lightw. Technol.,* vol. 17, no. 12, pp. 2542-2550, 1999.

[19] K. L. Hall, G. Lenz, A. M. Darwish, and E. P. Ippen, "Subpicosecond gain and index nonlinearities in InGaAsP diode lasers," *Opt. Comm.,* vol. 111, no. 5-6, pp. 589-612, 1994.

[20] M. J. Connelly, "Wideband semiconductor optical amplifier steady-state numerical model," *IEEE J. Quantum Electron.,* vol. 37, no. 3, pp. 439-447, 2001.

[21] B. R. Bennett, R. A. Soref, and J. A. Del Alamo, "Carrier-induced change in refractive index of InP, GaAs and InGaAsP," *IEEE J. Quantum Electron.,* vol. 26, no. 1, pp. 113-122, 1990.

[22] L. A. Coldren and S. W. Corzine, *Diode lasers and photonic integrated circuits,* John Wiley & Sons, 1995.

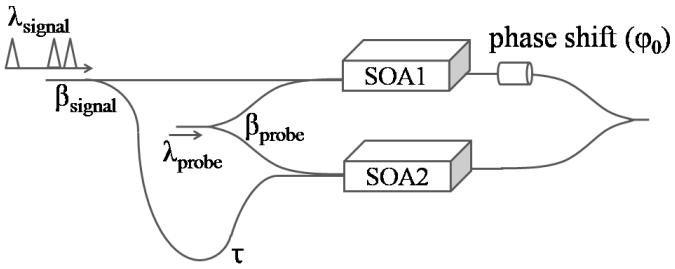


Fig.1. All-optical wavelength converter utilizing an active Mach-Zehnder interferometer. A longer optical path length preceding SOA2 provides the optical time delay, τ. The phase shift (ϕ_0) is considered a static design element.

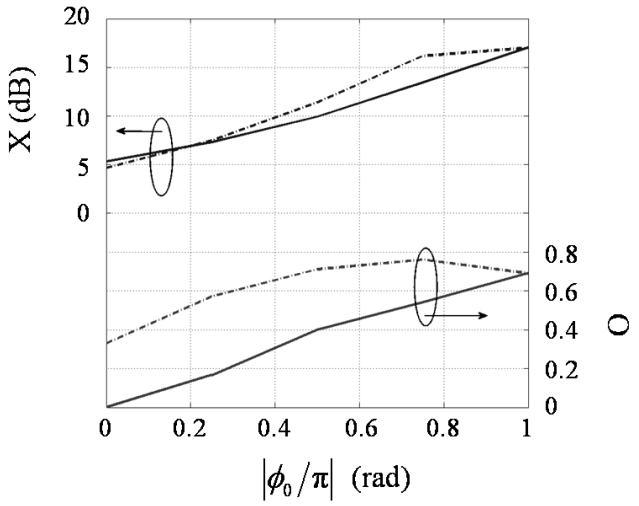


Fig. 2. Eye extinction (X) and opening (O) vs. static phase shift, ϕ_0. Dash-dot lines denote data taken by adjusting I_1 and using a $\phi_0 < 0$. Conversely, the solid lines describe the eye variation when I_2 is adjusted with $\phi_0 > 0$.

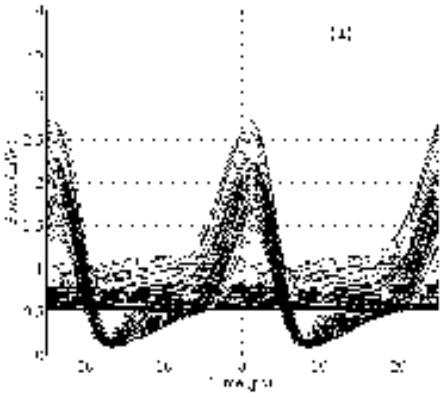


Fig. 3a. The best obtainable eye with $\phi_0 = 0$ when using symmetric power splitters and adjusting the current injection. No optical post-conversion filtering or detector electrical filtering is used and ASE noise is intentionally excluded from eye calculations. The eye diagrams display significant degradation from pattern effects even with optimized biasing.

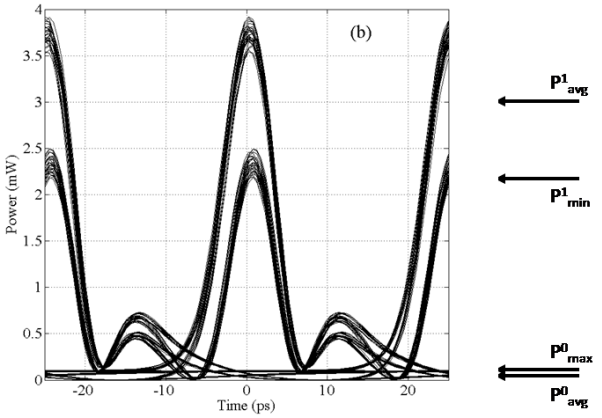


Fig. 3b. The best obtainable eye with $\phi_0 = \pi$ when using symmetric power splitters and adjusting the current injection. The power levels used in calculating the two eye parameters, X and O, are also shown.

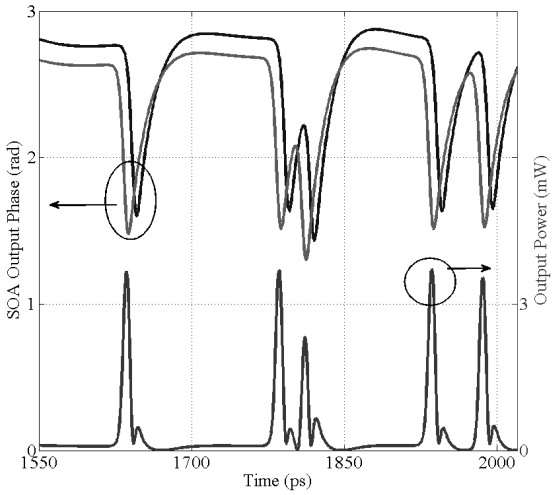


Fig. 4. Two SOA output phase responses are shown along with the output pulse intensity. The ~π phase shift between the two phase responses has been removed for clarity. Origins of trailing satellite pulses and poor zero-bit extinction can be seen.

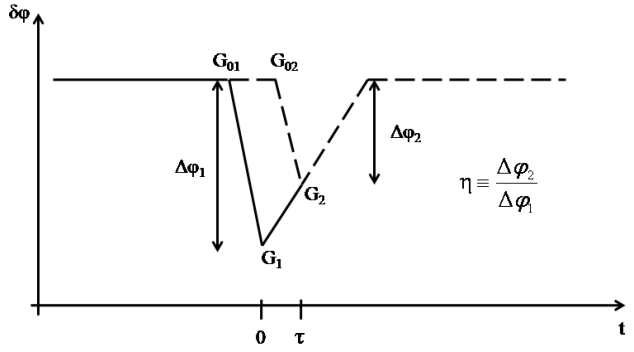


Fig. 5. Phase recoveries for the two SOAs. $\Delta\phi_{1,2}$ is the magnitude of the phase shift for SOA1,2 and τ is the temporal shift due to the optical delay preceeding SOA2.

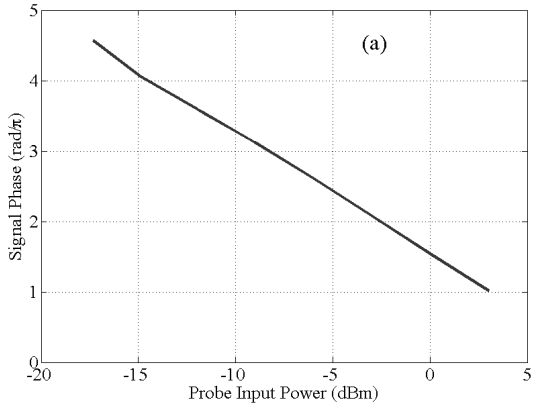


Fig. 6a. The phase evolution of the probe output while maintaining a constant output power, calculated without invoking an α-factor approximation. The constant slope suggests a single choice for β_{probe} will work consistently across a broad input power range. This is a graphical depiction of the behavior predicted by the simple relation of (1).

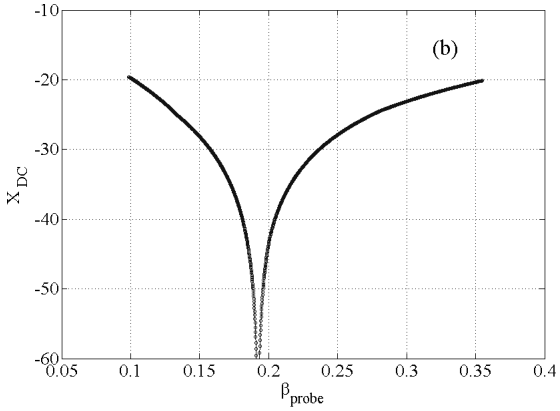


Fig. 6b. The variation in DC extinction with β_{probe}. Current injection is optimized at each data point.

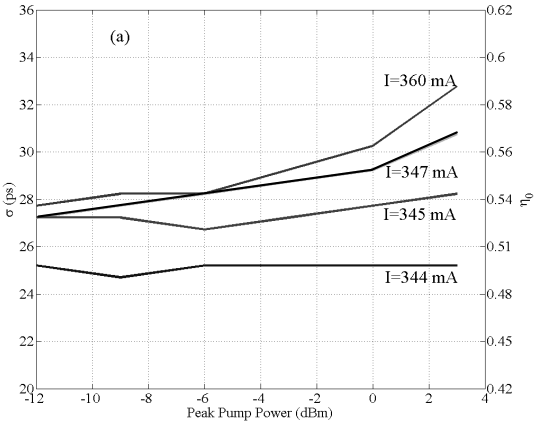


Fig. 7a. A plot of the probe (1547nm) phase recovery time (σ) vs the data signal (1567nm) pulse peak power. η_0 is calculated from σ using (4) and τ = 8ps. η_0 varies little across a large range of input pulse powers and SOA operating points. The input probe power is adjusted at each level of current injection to yield a constant probe output power.

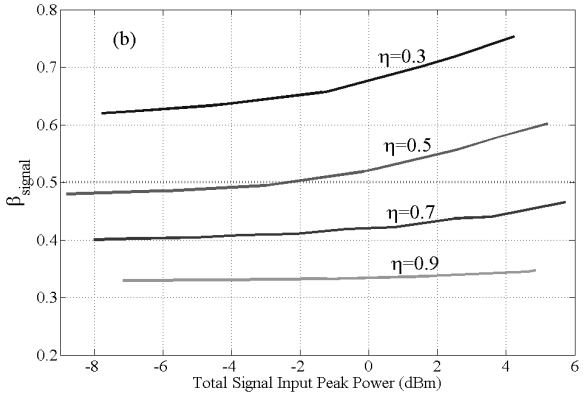


Fig. 7b. β_{signal} plotted along lines of constant η as a function of total input power to the signal splitter. For example, if a total signal input power of -2 dBm is input to the MZI, and $\eta_0 \approx 0.5$, the plot indicates a 50/50 power splitter should be utilized for the data signal.

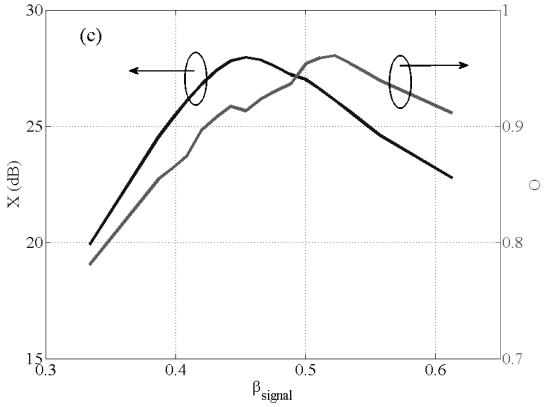


Fig. 7c. The variation of the eye extinction (X) and opening (O) with the signal power splitter, β_{signal}. Current bias is optimized at each data point.

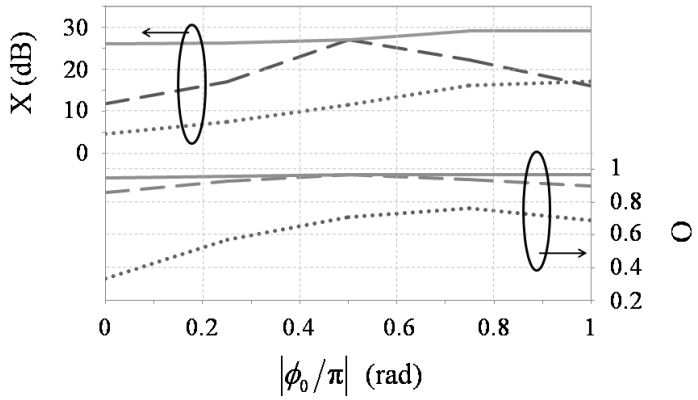


Fig. 8. The eye extinction (X) and opening (O) as a function of the static phase shift, ϕ_0. The dotted line depicts the data for symmetrical power splitters and is borrowed from Fig 2. The dash data shows the variation in eye performance for a converter optimized for operation at $\phi_0 = \pi/2$. The solid line illustrates the best converter performance when both power splitters are asymmetrically optimized for each value of ϕ_0. Note that $\phi_0 \geq 0$ for the asymmetrical converters and $\phi_0 \leq 0$ for the symmetrical MZI. Current bias is optimized for each data point.

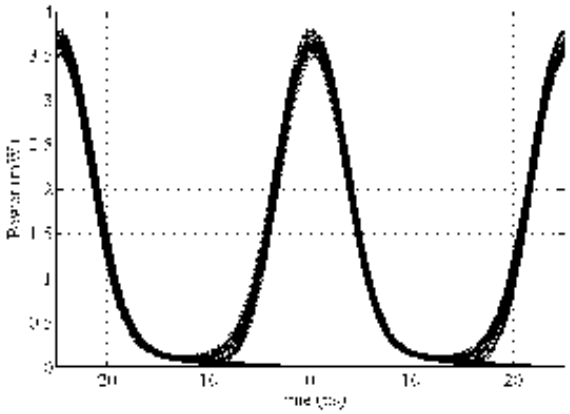


Fig. 9. Optimized asymmetrical MZI output eye with $\phi_0 = 0$.